Managing Charge Transport and Exciton Generation for Highly Efficient, Bright, and Stable Near-Infrared Organic Radical Light-Emitting Diodes

Hwan-Hee Cho, Min-Hsuan Chang, Yi-Syun Chen, Tetsuro Kusamoto, Emrys W. Evans, Yuh-Renn Wu*, Richard H. Friend**

Prof. Hwan-Hee Cho, Prof. Richard H. Friend
Cavendish Laboratory, Department of Physics, University of Cambridge, J J Thomson avenue, Cambridge, CB3 0HE, UK
E-mail: chohh@yonsei.ac.kr, rhf10@cam.ac.uk

Prof. Hwan-Hee Cho
Department of Materials Science and Engineering, Yonsei University, 50 Yonsei-ro, Seodaemun-gu, Seoul, 03722, Republic of Korea
E-mail: chohh@yonsei.ac.kr

Min-Hsuan Chang, Yi-Syun Chen, Prof. Yuh-Renn Wu
Graduate Institute of Photonics and Optoelectronics and Department of Electrical Engineering National Taiwan University, Taipei 10617, Taiwan
E-mail: yrwu@ntu.edu.tw

Prof. Tetsuro Kusamoto
(1) Department of Materials Engineering Science, Graduate School of Engineering Science, The University of Osaka, Toyonaka, Osaka 560-8531, Japan
(2) JST-FOREST, 4-1-8, Honcho, Kawaguchi, Saitama 332-0012, Japan.

Prof. Emrys W. Evans
Department of Chemistry, Swansea University, Singleton Park, Swansea, SA2 8PP

Keywords: organic radical, NIR OLEDs, doublet fluorescence, energy transfer, charge transport

Abstract

Near-infrared (NIR) organic light-emitting diodes based on open-shell radical emitters offer a spin-allowed pathway to high-brightness emission. However, their practical implementation has been hindered by efficiency roll-off at high current densities. Here, we demonstrate that simultaneously achieving balanced charge transport and high emission efficiency is key to overcoming this limitation in radical-based electroluminescence. By contrasting conventional exciplex-based reference systems with a thermally activated delayed fluorescence (TADF)-based architecture, we identify a trade-off between charge balance and photoluminescence efficiency arising from exciplex-mediated excitation pathways in radical electroluminescence. Leveraging efficient energy transfer from the TADF material while maintaining charge balance, we achieve a high external quantum efficiency of 8.1% at 804 nm, with over 5% EQE at a high current density of 100 mA cm^{-2}. Coupled Poisson and drift–diffusion modeling of device operation matches experimental observations and indicates that roll-off at high current densities is due primarily to quenching of doublet excitons by holes. This work establishes a TADF-assisted exciton management strategy for NIR radical electroluminescence and highlights its potential for next-generation NIR optoelectronic technologies.

1. Introduction

Near-infrared (NIR) organic electroluminescent devices operating beyond 800 nm have long faced a fundamental efficiency limitation. In conventional closed-shell organic emitters, the external quantum efficiency (EQE) rapidly decreases as the optical bandgap narrows because strong vibrational coupling in low-gap organic semiconductors exponentially exacerbates nonradiative decay, a phenomenon widely known as the energy gap law.[1] As a result, achieving EQEs exceeding ~5% in the NIR region has remained extremely challenging for typical organic light-emitting diodes (OLEDs).

Open-shell radical emitters, which exhibit doublet fluorescence, have recently emerged as a promising alternative to overcome this intrinsic limitation.[2–18] Unlike singlet–triplet systems, doublet emitters avoid the formation of nonradiative dark triplet excitons, thereby circumventing the statistical 1:3 singlet–triplet bottleneck that limits the radiative efficiency of conventional OLEDs.[19,20] Despite this conceptual advantage, translating doublet fluorescence into high-performance electroluminescence (EL) remains nontrivial. In particular, radical-based OLEDs suffer from pronounced efficiency roll-off and limited radiance and operational stability, which collectively hinder their practical deployment in NIR optoelectronic applications.

These challenges originate primarily from the unique electronic structure of the triphenylmethyl organic radicals that have been primarily studied. Owing to their intrinsically low-lying singly occupied molecular orbitals (SOMOs), radical emitters act as strong electron traps when dispersed in conventional wide-gap host matrices, which must be selected to have a triplet exciton energy no lower than the doublet exciton supported by the radical. This charge trapping leads to the accumulation of electrons and excitons near the interface between the emissive layer (EML) and the electron transport layer (ETL), where nonradiative quenching processes, such as exciton–exciton annihilation, are significantly intensified.[21] Consequently,

even though doublet fluorescence can suppress spin-forbidden losses, device-level performance becomes limited by spatially localized recombination and associated nonradiative loss processes, resulting in rapid efficiency roll-off at high current densities, reduced radiance, and compromised stability.

To mitigate these issues, exciplex-forming mixed-host architectures have been designed and explored to improve charge balance within the EML.[10] While such approaches can effectively enhance electron transport and suppress efficiency roll-off, they introduce a new trade-off: the emissive efficiency of the radical system is significantly reduced when excitons are generated or transferred through low-efficiency and slowly decaying exciplex states. This trade-off between charge-transport optimization and emissive efficiency has thus limited the achievable performance of radical-based NIR OLEDs, indicating that further progress requires a different device design paradigm that circumvents the trade-off between charge balance and exciton generation efficiency.

In this work, we elucidate the interdependent roles of charge transport, exciton generation, and radiative efficiency in radical-based NIR OLEDs. We first investigate a mixed-host strategy aimed at enhancing electron transport in the EML and clarify its impact on efficiency roll-off and high-current-density operation. However, we demonstrate that despite improved charge transport, exciplex-mediated exciton generation results in a pronounced reduction in doublet fluorescence quantum efficiency, thereby constraining the overall EL efficiency. To overcome this limitation, we introduce a green thermally activated delayed fluorescence (TADF) host that provides an auxiliary exciton-harvesting pathway while simultaneously improving charge balance to enable efficient radical EL. By comparing exciplex- and TADF-based device architectures, we reveal that improving charge balance alone is insufficient to sustain high EL performance, as exciton generation through low-efficiency

intermediates severely reduces doublet-emission efficiency. In contrast, the TADF-based architecture reconciles charge balance with efficient exciton harvesting, enabling the achievement of substantially enhanced radiance, suppressed efficiency roll-off, and improved operational stability. Detailed photophysical characterization and device modeling further clarify the emission mechanism and the origin of efficiency roll-off in radical OLEDs, providing critical design insights for high-performance NIR doublet EL.

2. Results and Discussion

2.1. Charge control in radical electroluminescent devices

As charge trapping has been identified as a major origin of efficiency roll-off in radical OLEDs, we first examine exciplex-based radical EL systems in which electron transport is deliberately enhanced. It was shown that a mixed host system comprising 4,4′,4″-tris(carbazol-9-yl) triphenylamine (TCTA) and bis-4,6-(3,5-di-3-pyridylphenyl)-2-methylpyrimidine (B3PYMPM) in a 1:1 ratio boosted the performance of radical EL devices at high current densities.[10] In the current study, we replaced B3PYMPM with 4,6-bis[3,5-(dipyrid-4-yl)phenyl]-2-methylpyrimidine (B4PYMPM) in both the mixed host and the electron transport layer (ETL) to enhance electron transport in devices, since B4PYMPM was reported to have an order-of-magnitude higher electron mobility than B3PYMPM (1.0×10^{-4} cm^2 V^{-1} s^{-1} vs. 1.5×10^{-5} cm^2 V^{-1} s^{-1}).[22,23] As a control host, 4,4-bis(carbazol-9-yl)biphenyl (CBP) was employed because its wide energy gap and adequate charge-transporting properties make it a well-established reference host for radical-based OLEDs.[3,7–10] The chemical structures of the materials used in these emissive systems are depicted in **Figure 1**a. Figure 1b illustrates the device architecture, along with an energy diagram of the charge transport and emissive layers. A hole transport layer (HTL) consisted of TAPC and TCTA with thicknesses of 30 nm and 10 nm, respectively, and B4PYMPM was employed as an ETL with a thickness of 80 nm. As a

radical emitter, the 800 nm emissive TPA-PyBTM'[10,17] was doped into CBP and TCTA:B4PYMPM hosts with a 3% doping concentration. The two devices were fabricated by vacuum deposition, and their optoelectronic performance is displayed in Figure 1c~e and summarized in **Table 1** (see also Table S1 and Figure S1 for device reproducibility).

Table 1. Summary and comparison of device performance on CBP and mixed host devices.

EML	V_{on} [a)] (V)	EQE_{Max} (%)	$EQE_{J\text{-}1}$ [b)] (%)	$EQE_{J\text{-}10}$ [c)] (%)	$EQE_{J\text{-}100}$ [d)] (%)	$Radiance_{Max}$ (mW sr^{-1} m^{-2})	λ_{max} (nm)
CBP:TPA-PyBYM' 3%	3.2	6.2	4.0	1.8	0.4	1,800	810
TCTA:B4:TPA-PyBYM' 3%	2.4	5.7	4.6	4.1	2.7	41,000	814

[a)]Voltage at 10^{-1} mW sr^{-1} m^{-2}, [b)]EQE at 1 mA cm^{-2}, [c)]EQE at 10 mA cm^{-2}, [d)]EQE at 100 mA cm^{-2}

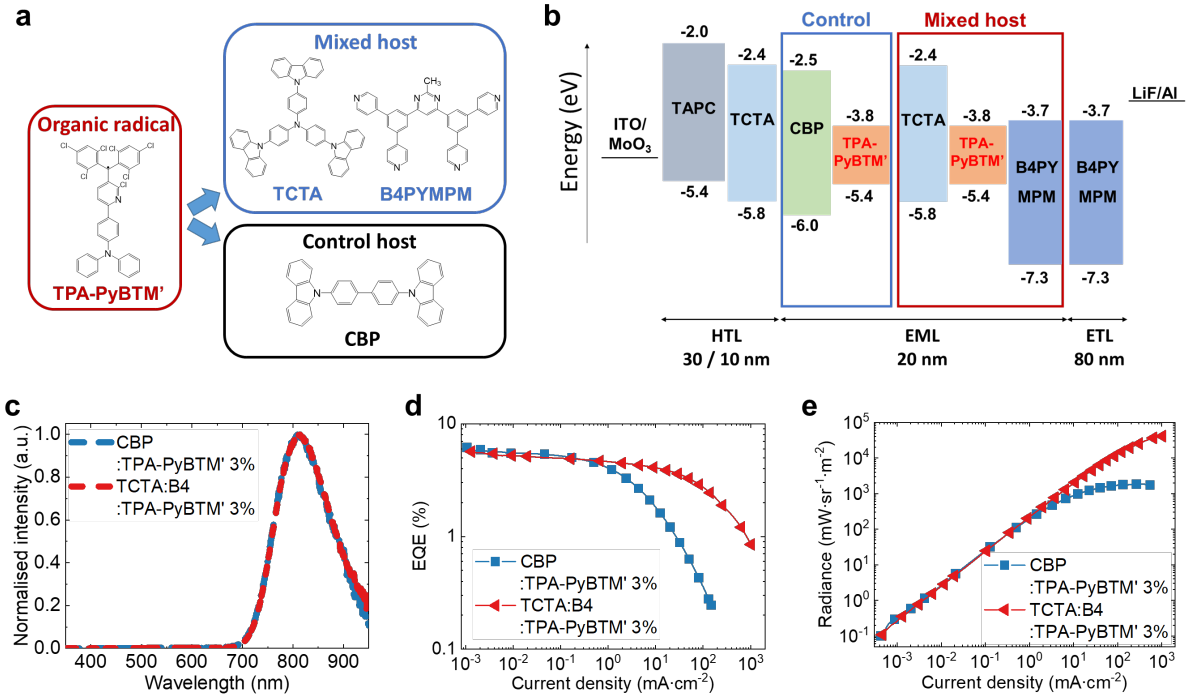


Figure 1. Optoelectronic characteristics of radical EL devices using the wide-gap control and mixed hosts. a) Chemical structures of TPA-PyBTM', TCTA, B4PYMPM, and CBP. b) Device architecture and energy level diagram. c) EL spectra at 1 mA cm^{-2}. d) EQE-current density plots. e) Radiance-current density plots.

Figure 1c shows the EL spectra of the devices measured at a current density of 1 mA cm^{-2}. Both devices exhibit pure near-infrared emission with a peak wavelength of approximately 810 nm. The corresponding EQE characteristics are presented in Figure 1d. The

TCTA:B4PYMPM device reaches a maximum EQE of 5.7%, which is slightly lower than that of the CBP-based control device (6.2%). Although the TCTA:B4PYMPM device does not show a higher peak EQE than the CBP-based control, it exhibits superior overall EL performance (see also the EQE–radiance characteristics in Figure S2).

Owing to the enhanced electron transport afforded by B4PYMPM, a low driving voltage of 2.4 V is achieved (Table 1 and Figure S3). More importantly, the efficiency roll-off is markedly suppressed, enabling a high maximum radiance of 41,000 mW sr^{-1} m^{-2}, which is more than an order of magnitude higher than that of the CBP device (1,800 mW sr^{-1} m^{-2}). These improvements correlate with the voltage-dependent EL spectra. The CBP-based device exhibits a pronounced blue shift at higher voltages due to the emergence of interfacial exciplex emission (Figure S4), indicating a narrow recombination zone near the EML/ETL interface that promotes exciton quenching.[9] In contrast, the TCTA:B4PYMPM device maintains stable EL spectra over the entire voltage range (Figure S5), consistent with enhanced electron transport and an expanded emission zone within the EML. In addition, operational lifetime measurements performed at 0.1 mA cm^{-2} (Figure S6) reveal that the TCTA:B4PYMPM device exhibits a lifetime approximately 120 times longer than that of the CBP-based device (48.4 h versus 0.4 h at 50% EL decay).

To clarify the origin of the improved performance observed in the TCTA:B4PYMPM device relative to the CBP-based control, additional electrical and spectroscopic analyses were conducted. Single-carrier devices were fabricated (see Figure S7 for the device structure), and their J–V characteristics were compared for the control and exciplex-based devices (Figure S8). As expected, both hole-only and electron-only devices (HODs and EODs) based on TCTA:B4PYMPM exhibit significantly enhanced charge transport relative to those based on CBP, consistent with the improved EL performance of the exciplex device, particularly at high current densities. In addition, the enhanced EL performance compared with previously reported

B3PYMPM-based devices can be attributed to the superior electron-transporting properties of B4PYMPM relative to B3PYMPM, as demonstrated in Figure S9. Meanwhile, J-V curves of both HODs and EODs for the control and exciplex devices become shallower when radicals are doped into the hosts, indicating that radical doping causes considerable charge trapping. This supports direct doublet exciton generation at radical sites through charge trapping as a major excitation pathway under device operation. To further probe the emission processes, transient EL and magneto-EL (MEL) measurements were performed. The rapid decay of doublet EL in the TCTA:B4PYMPM device indicates that direct doublet exciton generation at radical sites dominates the EL process rather than host-to-guest energy transfer (Figure S10). Nevertheless, a minor contribution from energy transfer is evident in the positive MEL response (Figure S11), suggesting the coexistence of multiple excitation pathways: exciplex-mediated energy transfer to the radical and direct doublet exciton generation at radical sites.[9]

Photophysical characterization provides critical insight into the origin of the limited device efficiency (key photophysical parameters are summarized in Tables S2 and S3). Fundamental steady-state photophysical characteristics of the hosts and radical emitter were first examined, as shown in Figures S12-S14; the PL characteristics of TCTA, B4PYMPM, and their blend confirm exciplex formation in TCTA:B4PYMPM (Figure S13). The photoluminescence quantum efficiency (PLQE) of the exciplex:TPA-PyBTM' blend is substantially reduced compared to that of the CBP:TPA-PyBTM' blend (8% vs. 21%, shown in Table S3), in agreement with previous observations for B3PYMPM-based mixed hosts.[10] The formation of intermolecular charge-transfer excitons in the exciplex significantly slows the exciton decay rate compared to that in wide-gap host components (see Figure S15 for transient PL characteristics), leading to a large reduction in the Förster resonance energy transfer (FRET) rate (from ~10^{10} s^{-1} to ~10^{7} s^{-1}, see Table S3). As a result, substantial energy loss occurs during exciton formation and subsequent energy transfer from the exciplex to the radical emitter.

Notably, despite the substantial decrease in PLQE from 21% to 8%, the maximum EQE remains comparable for the CBP- and exciplex-based devices (5.7% and 6.2%, respectively). This discrepancy between the PLQE and EQE trends can be attributed to the different exciton-generation pathways under optical and electrical excitation. Under electrical excitation, charge trapping by the radical enables direct doublet exciton generation, as supported by the single-carrier and transient EL measurements, thereby bypassing the inefficient exciplex-to-radical energy-transfer pathway that strongly affects the PLQE. In addition, the enhanced charge transport in the TCTA:B4PYMPM mixed host facilitates more balanced electrical excitation, partially compensating for the reduced radiative efficiency of the exciplex-based system. These results highlight an inherent trade-off in the exciplex-based system: enhanced charge transport improves high-current-density operation and mitigates efficiency roll-off, whereas inefficient exciplex-to-radical energy transfer limits the attainable emission efficiency.

2.2 Green TADF host:radical guest design

The limitations identified in exciplex-based radical EL systems motivate the development of an alternative host–guest design that preserves efficient charge transport while mitigating energy loss associated with exciplex-mediated exciton formation and transfer. To address this challenge, we introduce a TADF material as a single host for the radical emitter to provide efficient exciton harvesting and balanced charge transport without relying on intermolecular exciplex formation. An efficient green TADF material, 9,10-bis(4-(9H-carbazol-9-yl)-2,6-dimethylphenyl)-9,10-diboraanthracene (CzDBA) (the chemical structure is shown in Figure 3), was selected as the host due to its high PLQE (>90%) in neat films and bipolar charge-transporting characteristics.[24,25] These properties are expected to facilitate both

efficient energy transfer to the radical emitter and balanced carrier injection within the emissive layer.

Figure 2 schematically compares the excitation and emission processes in the green exciplex-based and green TADF-based radical systems. In the exciplex-based system, although nearly barrier-free charge injection enables efficient direct formation of doublet excitons at radical sites, exciton generation via intermolecular exciplex states is inefficient, leading to energy loss during the EL process. In contrast, the green TADF-based system promotes balanced direct exciton formation at the radical while providing an additional exciton-harvesting pathway from the TADF host, in which only intramolecular charge-transfer excitons are involved. In addition, the incorporation of appropriate blocking layers improves exciton confinement within the EML and suppresses charge leakage, thereby contributing to reduced efficiency roll-off at high current densities.

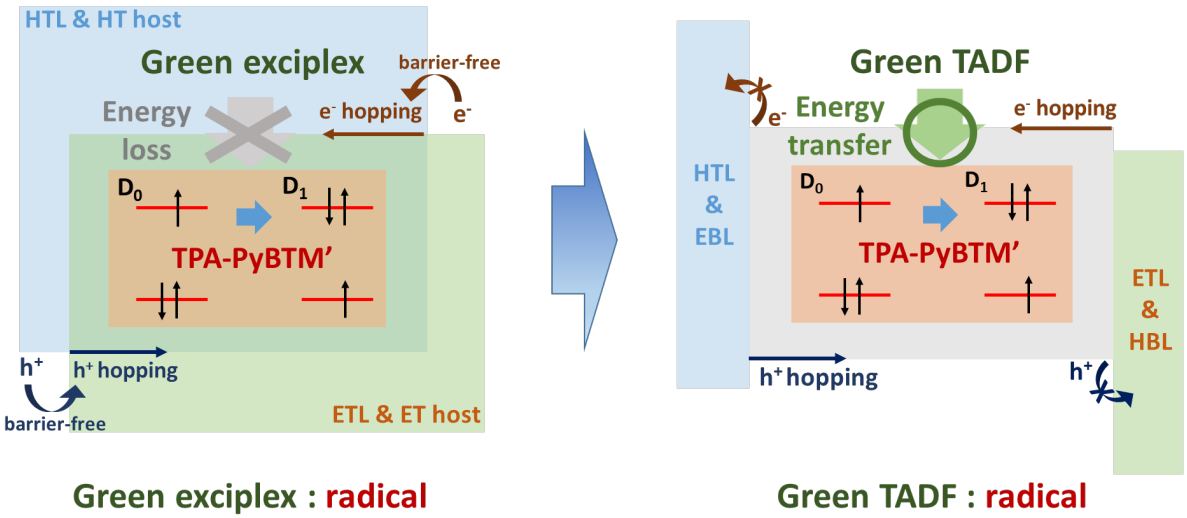


Figure 2. Conceptual illustration of the exciton-generation pathways in exciplex- and TADF-based radical OLEDs. The exciplex-based architecture facilitates balanced charge transport through barrier-free charge injection but suffers from substantial energy loss during exciplex-mediated energy transfer, limiting doublet-emission efficiency. In contrast, the TADF-based architecture enables efficient energy transfer to the radical emitter while excitons are effectively confined within the emissive layer by the blocking layers, thereby reconciling balanced charge transport with efficient exciton generation.

Steady-state and transient photophysical measurements were performed on radical-doped and nondoped CzDBA films under 330 nm laser excitation. **Figure 3**a presents the

steady-state photophysical properties of the CzDBA-based system. As the absorption spectrum of TPA-PyBTM' broadly spans from the ultraviolet (UV) to the green region, the spectral overlap between the CzDBA photoluminescence (PL) and the absorption of TPA-PyBTM' facilitates efficient energy transfer from CzDBA to the radical emitter. The CzDBA emission is not fully quenched under optical excitation, likely due to the relatively low radical-doping concentration (3%), consistent with the behavior observed in previous work[9,10] and with the PL spectra of the CBP- and TCTA:B4PYMPM-based blends, as shown in Figure S14. Moreover, the PLQE of the CzDBA:TPA-PyBTM' film reaches 26%, which is significantly higher than that of exciplex:TPA-PyBTM' systems (PLQE <10%), demonstrating that the energy loss associated with exciplex-mediated excitation is largely mitigated in the TADF-based system.

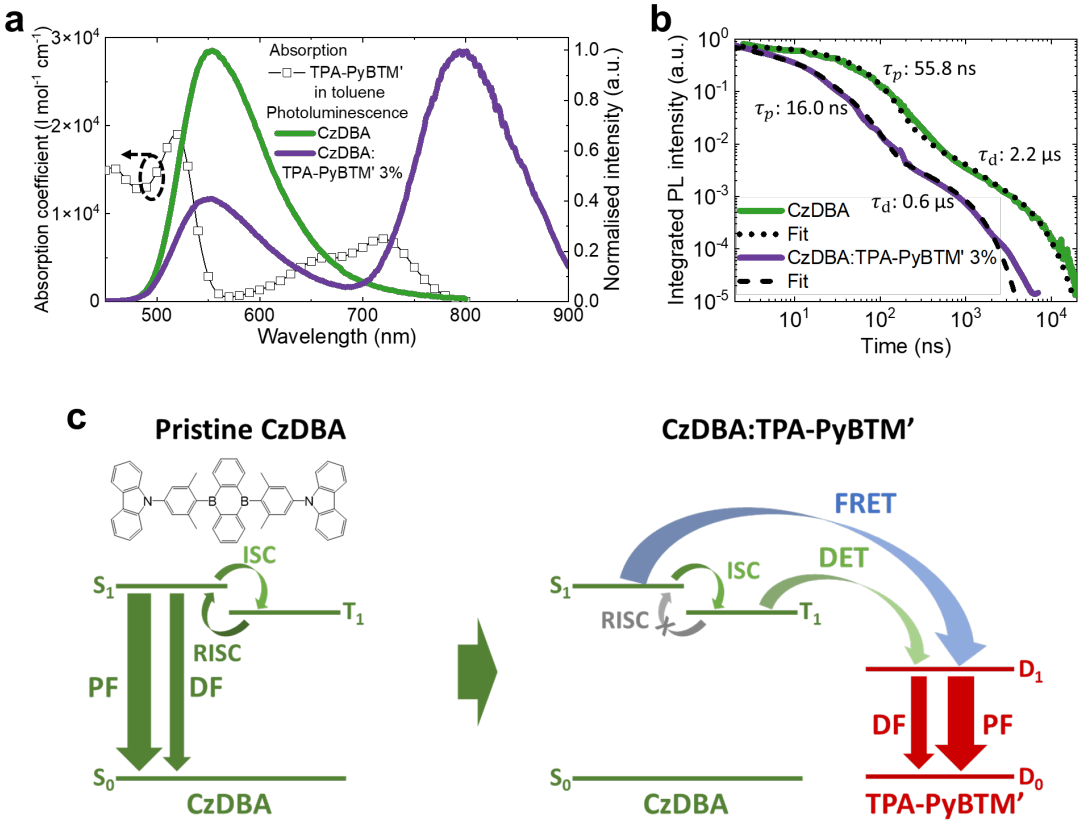


Figure 3. Steady-state and transient thin-film photophysics; the PL measurements were performed using 330 nm excitation. a) Absorption coefficient of TPA-PyBTM' and PL spectra of CzDBA neat and CzDBA:TPA-PyBTM' 3% films. b) Transient PL curves for CzDBA neat and CzDBA:TPA-PyBTM' 3% films. c) Schematic representation of the emission mechanisms for CzDBA TADF and CzDBA:TPA-PyBTM' doublet fluorescence systems.

Next, transient PL measurements were performed on pristine CzDBA and radical-doped CzDBA films to investigate the emission mechanism and energy transfer processes in the CzDBA-based system (Figure 3b). As illustrated in Figure 3c, the delayed emission observed in pristine CzDBA originates from intersystem crossing and subsequent reverse intersystem crossing (ISC and RISC). In contrast, in the CzDBA:TPA-PyBTM' system, efficient Dexter energy transfer (DET) from the CzDBA triplet state to the TPA-PyBTM' doublet state can occur. Upon doping TPA-PyBTM' into CzDBA, the transition from prompt to delayed emission occurs at an earlier time compared to pristine CzDBA (see also Figure S16 for a comparison of the integrated PL intensity). This observation suggests that the delayed doublet fluorescence primarily arises from ISC followed by DET, rather than from ISC/RISC followed by FRET.[9,12,14] If the delayed doublet emission were dominated by delayed FRET, analogous to TADF-sensitized fluorescence (so-called hyperfluorescence), the onset of delayed emission would closely resemble that of pristine CzDBA, resulting in a similar transient PL profile.[26,27] The distinct transient PL characteristics observed here therefore indicate that both FRET and DET contribute to the doublet emission process in the CzDBA:TPA-PyBTM' system.[9,12] A detailed analysis of exciton decay and energy transfer pathways is provided in Supporting Information S2-1, and important photophysical parameters are summarized in Table S4.

2.3 High-performing doublet fluorescent NIR OLEDs

Building on the optimized exciton management and charge-transport strategy discussed above, we next evaluate the EL performance of NIR OLEDs employing the CzDBA:TPA-PyBTM' emissive system. Devices were fabricated by vacuum deposition, and their optoelectronic characteristics are summarized in **Figure 4** and **Table 2** (see also Table S5 and Figure S17 for device reproducibility). The device architecture is illustrated in Figure 4a. As shown schematically in Figure 2, the EML is sandwiched between a high-energy HTL (1,3-

bis(N-carbazolyl) benzene, mCP) and a deep-energy-level ETL (B4PYMPM). This device-engineering strategy can further optimize device performance by suppressing efficiency roll-off at high current densities and enhancing radiance, as demonstrated in our previous work.[9] The radical emitter was hosted in CzDBA at a doping concentration of 3%. Figure 4b presents the EL spectrum of the device, which shows pure NIR emission with a peak at 804 nm, consistent with that shown in Figure 1c (see also Figure S18 for voltage-dependent EL spectra). CzDBA emission is almost completely quenched under electrical excitation, indicating that the dominant emission pathway depends strongly on the exciton generation mechanism.[8–10] To directly compare the emission behaviors under optical and electrical excitation, the normalized PL and EL spectra are presented in Figure S19. Under optical excitation, residual CzDBA emission is observed in the PL spectrum, indicating incomplete energy transfer from CzDBA to the radical emitter. In contrast, CzDBA emission is almost completely absent from the EL spectrum, suggesting that the excitation pathway under electrical operation differs from that under optical excitation. Although excitons may be generated on both CzDBA and the radical under electrical excitation, the negligible CzDBA emission is consistent with direct doublet exciton generation at radical sites being the dominant EL pathway. This interpretation is further supported by the transient EL and MEL measurements discussed below. The J-V-radiance characteristics and EQE as a function of current density are shown in Figures 4c and 4d, respectively (see also Figure S20 for the EQE-radiance graph). A maximum radiance of 70,800 mW sr^{-1} m^{-2} and a peak EQE of 8.1% were achieved. Compared to the exciplex-based reference device, the green TADF-based device exhibits a >40% higher maximum EQE and a >70% higher maximum radiance. As summarized in Table S6, this combination of high EQE and radiance represents excellent overall performance among reported NIR OLEDs operating in the 800–900 nm spectral range.

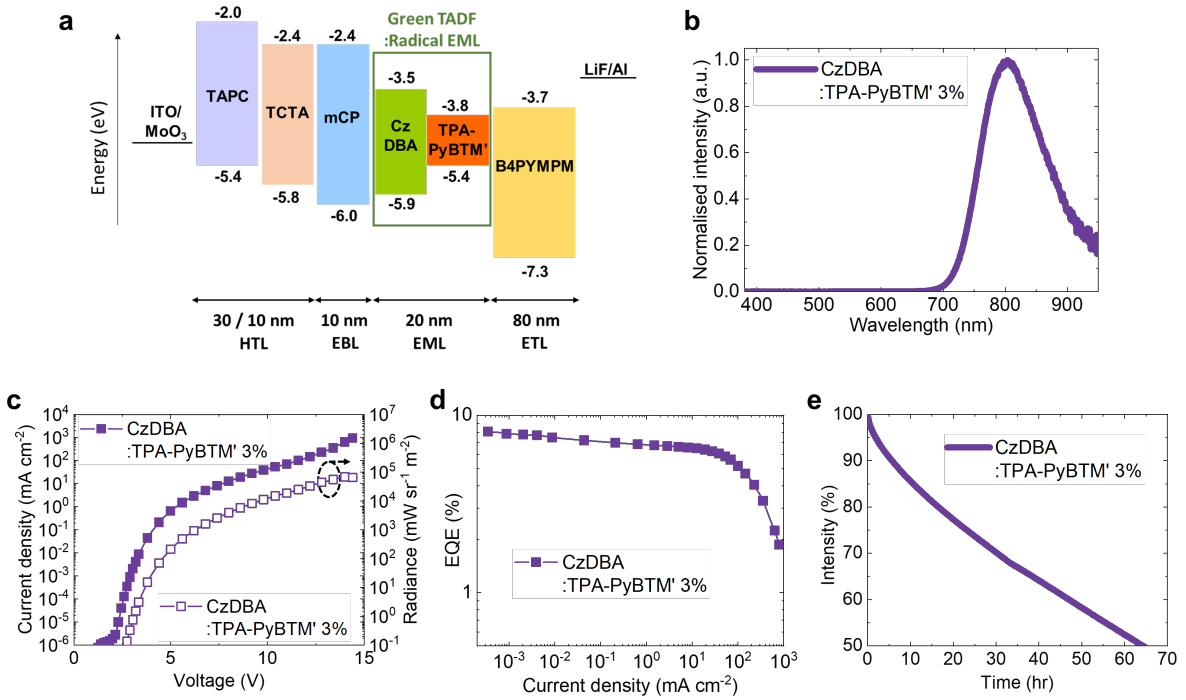


Figure 4. Optoelectronic characterization of CzDBA:TPA-PyBTM' OLED. a) Device structure with energy levels. b) EL spectrum measured at 1 mA cm^{-2}. c) Current density-voltage-radiance plots. d) EQE-current density plot. e) Device lifetime measured at 0.1 mA cm^{-2}.

Table 2 | Summary of device performance.

	V_{on}[a)] (V)	EQE_{Max} (%)	$EQE_{J\text{-}1}$[b)] (%)	$EQE_{J\text{-}10}$[c)] (%)	$EQE_{J\text{-}100}$[d)] (%)	$Radiance_{Max}$ (mW sr^{-1} m^{-2})	λ_{max} (nm)
CzDBA:TPA-PyBTM' 3%	2.7	8.1	6.8	6.5	5.2	70,800	804

[a)]Voltage at 10^{-1} mW sr^{-1} m^{-2}, [b)]EQE at 1 mA cm^{-2}, [c)]EQE at 10 mA cm^{-2}, [d)]EQE at 100 mA cm^{-2}

Importantly, the device shows considerably suppressed efficiency roll-off: more than 80% of the maximum EQE is retained at a high current density of 10 mA cm^{-2}, and even at 100 mA cm^{-2}, an EQE of 5.2% (>60% of the maximum EQE) is maintained. These values surpass those of previously reported radical-based OLEDs in terms of efficiency retention under high-current-density operation.[8–10] Operational lifetime measurements (Figure 4e) demonstrate further enhanced device stability, with a lifetime of approximately 65 h, representing a ~35% improvement over the exciplex-based device discussed above. Overall, the CzDBA:TPA-PyBTM' device exhibits substantially superior EL performance relative to

exciplex-based counterparts, ranking among the highest-performing NIR OLEDs operating at 800 nm and beyond.[8]

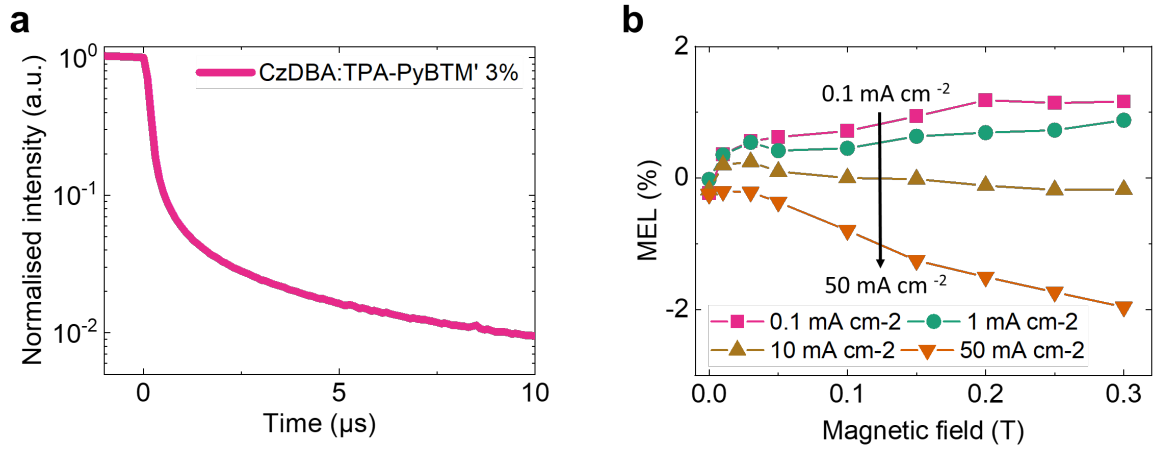


Figure 5. Transient EL and MEL profiles for CzDBA:TPA-PyBTM' OLED. a) Transient EL plot at 5 V at a frequency of 20,000 Hz and a pulse width of 10 μs. b) MEL plots from 0.1 to 50 mA cm^{-2}. MEL is defined as: MEL (%) = [EL(B)-EL(0)]/EL(0), where EL(B) and EL(0) are the EL intensities in the presence and absence of a magnetic field, B, respectively.

To probe the EL mechanisms, transient EL and MEL measurements were performed, as shown in **Figure 5**. The transient EL response (Figure 5a) exhibits rapid doublet fluorescence without delayed emission components, similar to that observed in exciplex-based radical devices, indicating that direct doublet exciton generation at radical sites is the dominant emission pathway. An emission spike or additional emission after turn-off, which can arise from unbalanced charge trapping and accumulation within the EML or at its interfaces,[28,29] was not observed, consistent with the improved charge balance in the CzDBA-based device. Thus, even when excitons are primarily generated via charge trapping, exciton quenching can be effectively suppressed at high current densities through improved charge balance.[9] This interpretation is also supported by single-carrier device analysis, with the corresponding device structure and J–V characteristics shown in Figures S21 and S22. The single-carrier characteristics indicate more balanced hole and electron transport in the CzDBA-based device than in the exciplex-based device, as evidenced by the lower HOD current together

with their comparable EOD characteristics. This improved charge balance can reduce excessive charge and exciton accumulation near the EML/ETL interface, thereby contributing to the simultaneous enhancement of efficiency, radiance, and operational stability.

Although the transient EL does not display a pronounced delayed component associated with triplet-to-doublet energy transfer, triplet excitons generated in the host are still expected to contribute to the emission process. This contribution is confirmed by MEL measurements (Figure 5b), which show a positive MEL response at low current densities (≤ 10 mA cm^{-2}), indicative of triplet-to-doublet DET, consistent with the delayed component observed in transient PL (Figure 3b) and with previous reports.[9,12] These results indicate that EL in the present devices originates from a combination of balanced-transport-enabled direct doublet exciton formation at radical sites and TADF-assisted triplet-to-doublet energy transfer, both of which contribute to the high efficiency and radiance of the devices.

At higher current densities, however, the MEL signal transitions from positive to negative. This behavior suggests that, while DET contributes to the EL process at low current densities, an increased triplet exciton population at high current densities promotes triplet–triplet annihilation (TTA) and triplet–polaron quenching (TPQ), which outcompete DET and lead to a negative MEL response.[9,30] These observations indicate that efficiency roll-off at high current densities in this emissive system originates from multiple competing energy-loss processes, including TTA, TPQ, and doublet polaron quenching (DPQ). The roles of charge transport, exciton generation, and exciton quenching in efficiency roll-off are investigated in the following section through device modeling.

2.4. Device modeling

Device simulations were performed using a two-dimensional finite element method (FEM)-based framework that solves the coupled Poisson and drift–diffusion equations, together

with an exciton diffusion solver incorporating three exciton species, which is a widely adopted approach for modeling the electrical characteristics of OLEDs.[31,32] In this study, the Poisson and drift–diffusion framework is integrated with a Gaussian density-of-states (DOS) model and field-dependent carrier mobility to simulate charge transport in host–guest OLED systems while accounting for the effects of random dopant distributions (Figure S23).[33] Furthermore, a multi-exciton diffusion and energy-transfer model incorporating random dopant effects is employed to calculate the exciton distribution and internal quantum efficiency (IQE), providing insights into the mechanisms responsible for efficiency degradation. Detailed methodological information is provided in Supporting Information S3.

First, the J–V characteristics of EODs and HODs, with and without dopant incorporation, were fitted using the proposed model. The fitting results are shown in Figure S24, demonstrating good agreement with the experimental data after accounting for the effects of random dopant distributions. The extracted fitting parameters are summarized in Tables S7 and S8. Using the extracted mobility parameters, the J–V characteristics of the complete OLED device were simulated. The J-V characteristics of the OLED device with 3% dopant concentration are presented in Figure S25. A consistent trend is observed between the simulated and experimental J-V curves, indicating that the proposed model effectively captures charge transport behavior under low-doping conditions. Since holes have shallower trap levels and smaller injection barriers, the carriers predominantly recombine near the EML/ETL interface.

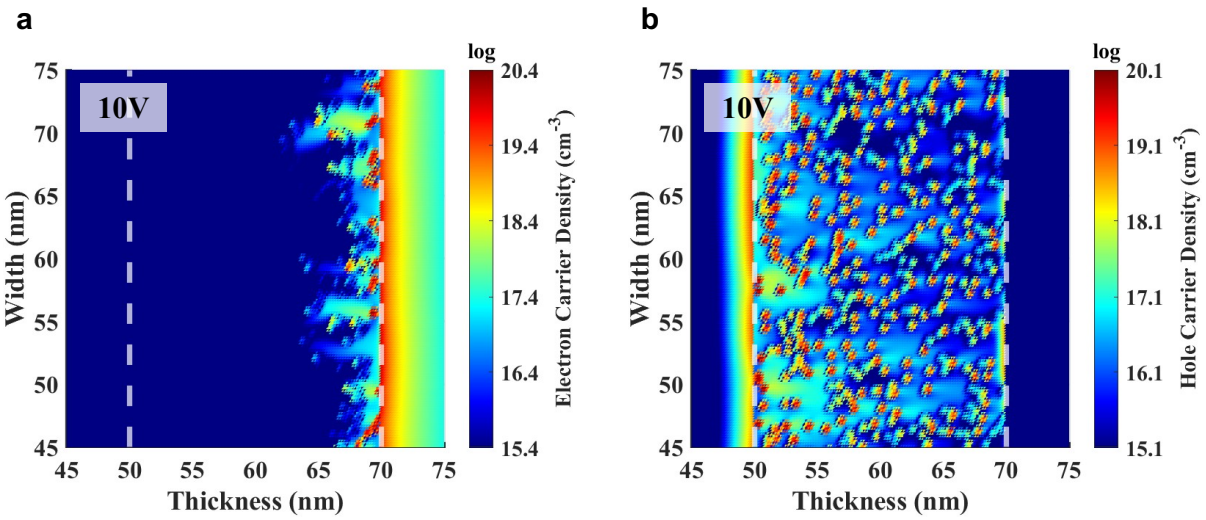


Figure 6. Carrier density maps in the EML under a 10 V bias, showing (a) electron and (b) hole distributions.

Figures 6a and 6b show the spatial distributions of accumulated electrons and holes within the emissive layer (EML), respectively (see also Figures S26 and S27 under different voltages and Figure S28 for hole and electron DOS). Both carriers exhibit localized accumulation during transport, reflecting charge trapping associated with random dopant distributions. In contrast to electrons, holes show a more spatially extended distribution, suggesting weaker trapping and higher effective hopping probability. Notably, these accumulation regions spatially coincide with the locations of the guest molecules, indicating that the deeper energy levels of the guest material act as charge traps, particularly under low-doping conditions.

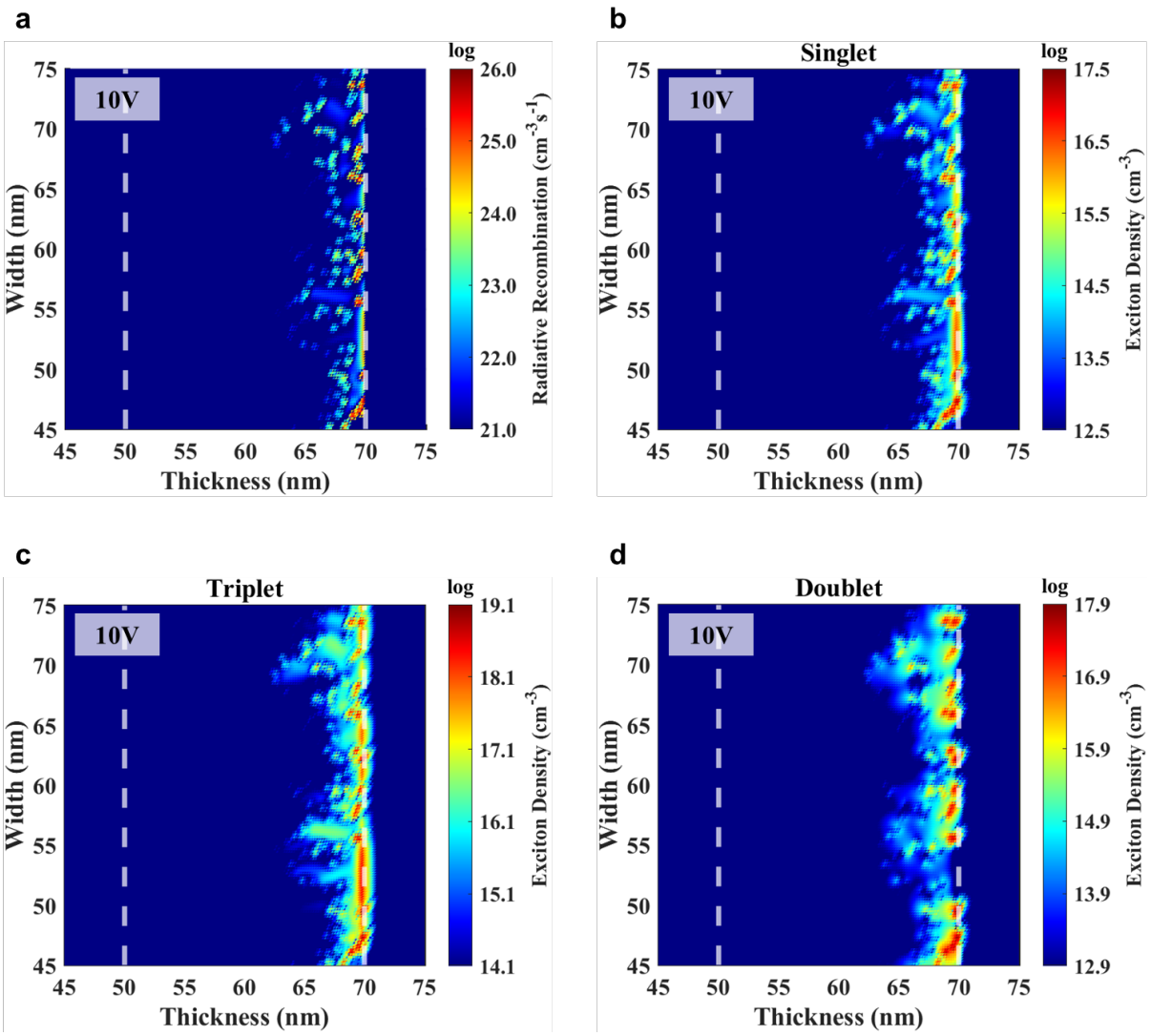


Figure 7. (a) Two-dimensional distribution of radiative recombination rates in the EML under an applied voltage of 10 V. (b–d) Exciton density maps in the EML under 10 V bias, showing spatial distributions of (b) singlet, (c) triplet, and (d) doublet excitons.

Figure 7a shows the spatial distribution of radiative recombination at an applied voltage of 10 V. The recombination zone is primarily localized in regions where both electrons and holes accumulate, suggesting that guest trap states may enhance the probability of radiative recombination. Figures 7b-d present the distributions of singlet, triplet, and doublet excitons within the EML under the same voltage, using the parameters summarized in Table S9. Excitons for all three types are primarily located near the guest material regions close to the EML/ETL interface, indicating that singlet and triplet excitons are largely able to transfer to guest states and form doublet excitons. Among the three, triplet excitons exhibit the highest density, likely due to their longer lifetime and higher generation probability, which facilitates accumulation

under continuous carrier injection. Owing to limited exciton diffusion, such high exciton densities can promote exciton–exciton annihilation and carrier-induced quenching processes (see also Figures S29-S32 for the distributions of quenching associated with doublet and triplet excitons).

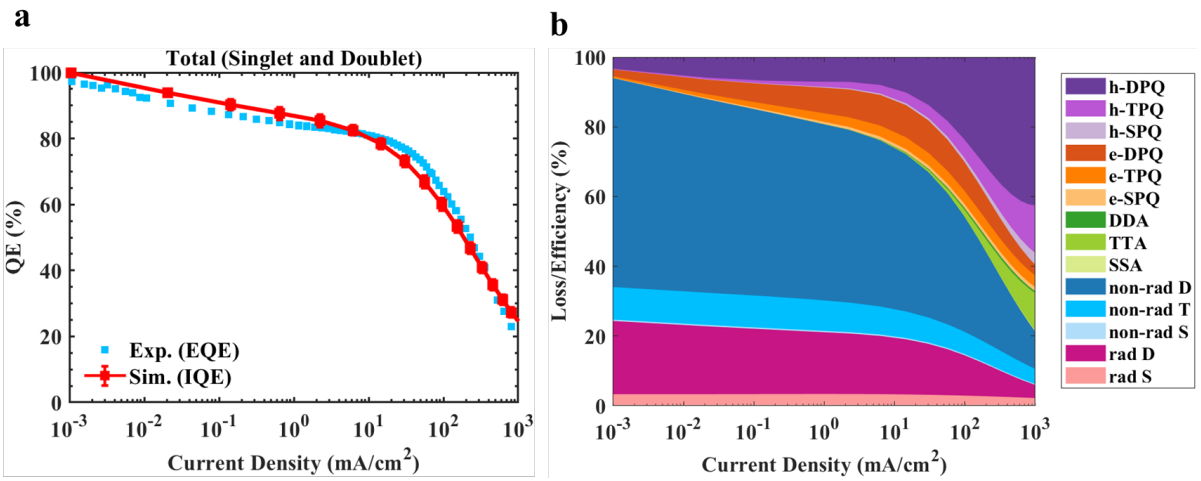


Figure 8. (a) Current density dependence of normalized simulated IQE and experimental external quantum efficiency (EQE). (b) Loss mechanisms across different current densities, categorized by singlet, triplet, and doublet excitons. The mechanisms include rad S, non-rad S, SSA, e-SPQ, h-SPQ, non-rad T, TTA, e-TPQ, h-TPQ, rad D, non-rad D, DDA, e-DPQ, and h-DPQ.

Figure 8a compares the normalized IQE from simulation and the normalized EQE measured experimentally as functions of current density. The simulated IQE closely follows the trend of the experimental EQE. The IQE curve exhibits two distinct regions separated by a threshold around 76.8 mA cm^{-2} (corresponding to 9 V). At lower current densities, the efficiency remains relatively stable, whereas a pronounced roll-off emerges at higher current densities. This roll-off is attributed to increased nonradiative loss processes, including hole-induced DPQ (h-DPQ) and TTA.

Figure 8b summarizes the radiative and nonradiative loss mechanisms based on the simulation results presented separately in Figures S33–S35, including radiative singlet (rad S), non-radiative singlet (non-rad S), singlet-singlet annihilation (SSA), electron-induced singlet-polaron quenching (e-SPQ), hole-induced SPQ (h-SPQ), non-radiative triplet (non-rad T), TTA,

electron-induced triplet-polaron quenching (e-TPQ), hole-induced TPQ (h-TPQ), radiative doublet (rad D), non-radiative doublet (non-rad D), doublet-doublet annihilation (DDA), electron-induced DPQ (e-DPQ), and h-DPQ. At low current densities, the efficiency is primarily limited by intrinsic nonradiative decay within the doublet channel, while both h-DPQ and e-DPQ act as secondary loss pathways contributing to the initial efficiency decrease. At high current densities, the loss landscape changes markedly. h-DPQ becomes the dominant loss pathway in the doublet channel, reflecting the rapid increase in hole density resulting from more efficient hole injection into the EML. e-DPQ also contributes noticeably at intermediate current densities (10 mA cm^{-2} ~ 100 mA cm^{-2}). Concurrently, h-TPQ and TTA increase with current density, indicating that polaron-exciton interactions and exciton-exciton annihilation become increasingly significant under high-injection conditions.

These non-radiative loss pathways substantially suppress emission efficiency at high current levels, leading to the pronounced efficiency roll-off observed experimentally. Moreover, the enhanced quenching and annihilation reduce the energy transfer efficiency from singlet and triplet excitons to doublet states, thereby weakening the radiative contribution of the doublet emission channel. Consequently, even though the CzDBA-based system significantly improves doublet EL performance compared to the exciplex- and CBP-based systems, energy loss due to exciton quenching and annihilation processes remains unavoidable, suggesting that future research should focus on minimizing these loss mechanisms to realize more optimized radical-based OLEDs.

3. Conclusion

In conclusion, this work demonstrates a viable strategy for realizing highly efficient, bright, and stable NIR OLEDs based on doublet fluorescence. By rationally managing charge transport and exciton generation, high EL efficiency can be sustained even at elevated current

densities by suppressing exciton annihilation processes that otherwise lead to severe efficiency roll-off. Compared with conventional exciplex-based systems, the TADF-based doublet-emissive architecture delivers markedly enhanced device performance through TADF-assisted exciton harvesting. As a result, a maximum EQE of 8.1% and a high radiance of 70,800 mW sr^{-1} m^{-2} are achieved, together with improved device lifetime. These performance gains are supported by comprehensive photophysical characterization and device-level analysis. Device modeling further elucidates the mechanisms underlying efficiency roll-off and exciton quenching, providing important insights into loss pathways that limit high-current-density operation and highlighting opportunities for continued optimization. The present TADF-based radical EL platform offers a promising route toward high-performance NIR OLEDs and is expected to find broad applicability in emerging technologies such as biosensing, bioimaging, optical communication, and surveillance.

Experimental Section

Sample preparation: To measure PL and absorption spectra in solution, TPA-PyBTM' was dissolved in toluene with 0.2 mg/ml. Organic films were made by a thermal evaporation process under high vacuum (~10^{-7} torr). 50 nm films of CBP, TCTA:B4PYMPM and CzDBA neat and TPA-PyBTM' 3% doped films were deposited on glass substrates to measure steady-state PL, PLQE, and transient PL. For the fabrication of OLEDs and single-carrier devices, ITO-coated substrates were cleaned with acetone and isopropyl alcohol, and then O_2 plasma treatment was applied to align the energy level with a hole transporting layer. All layers, including organic layers and a LiF/aluminum cathode, were thermally deposited under high vacuum (~10^{-7} torr). Doping concentrations used in films and devices are weight percentages.

Photophysical measurements: Steady-state PL spectra were measured by an Edinburgh Instruments fluorescence spectrometer (FLS980) with a monochromated xenon arc lamp at λ_{Ex}

= 330 nm under nitrogen flow. Shimadzu UV-3600 Plus spectrophotometer was employed for the measurement of absorption spectra. FLS980 with an integrating sphere under a nitrogen flow was used to measure PLQE, and the films were excited by a 330 nm laser. Transient PL was recorded by using an Andor electrically gated intensified charge-coupled device (ICCD) with 330 nm laser excitation; the decay kinetics were obtained from the integration of the total spectrum at each time.

Device characterization: The J-V characteristics of single-carrier devices were recorded by a Keithley 2635 source-meter. The performance of the OLED devices was measured by a Keithley 2635 source-meter and a calibrated Si photodiode. The EL spectra were recorded by an Ocean Optics Flame spectrometer. The device lifetime was measured using a calibrated Si photodiode that recorded EL intensity over time at a constant current density of 0.1 mA cm^{-1}. The devices were not encapsulated, and they were exposed to nitrogen twice during device fabrication due to changes in organic materials and a patterning mask for the Al cathode, which could detrimentally affect the device lifetime data. The transient EL characteristics are recorded by an Andor spectrometer setup (Andor SR303i) with an electrically gated ICCD camera (AndoriStar DH740 CCI-010). The voltage pulse was given by a Keithley 2401 function generator (20,000 Hz frequency and 10 μs pulse width). For MEL measurements, an EL device was positioned between magnet cores (GMW 3470 electromagnet), and a Keithley 2635 sourcemeter was utilized to apply the voltage to the device, and its EL spectrum was recorded by an Andor spectrometer (Shamrock 303i and iDus camera) with and without a magnetic field.

Device modeling methodology: The details are described in the Supporting Information.

Supporting Information

Supporting Information is available from the Wiley Online Library or from the author.

Data Availability Statement

The data that support the findings of this study are available from the corresponding author upon reasonable request.

Acknowledgements
H.-H.C. and R.H.F acknowledge funding from the ERC under the European Union's Horizon 2020 research and innovation program (grant agreement number 101020167). This research was supported by the Nano & Material Technology Development Program through the National Research Foundation of Korea (NRF) funded by Ministry of Science and ICT (RS-2026-25540008). This research was supported by the ANCHOR through the Seoul ANCHOR Center, funded by the Ministry of Education (MOE) and the Seoul Metropolitan Government. (2026-ANCHOR-01-022-04) Y.-R.W. is supported by the National Science and Technology Council, Taiwan, under grant No. NSTC 112-2221-E-002 -214 -MY3 and 115-2119-M-002-003 and by the Leap fellowship of the Foundation for the Advancement of Outstanding Scholarship.

Received: ((will be filled in by the editorial staff))
Revised: ((will be filled in by the editorial staff))
Published online: ((will be filled in by the editorial staff))

References

[1] A. Zampetti, A. Minotto, and F. Cacialli, "Near-Infrared (NIR) Organic Light-Emitting Diodes (OLEDs): Challenges and Opportunities," *Advanced Functional Materials* 29 (2019): 1807623, https://doi.org/10.1002/adfm.201807623.

[2] H. Guo, Q. Peng, X.-K. Chen, et al., "High Stability and Luminescence Efficiency in Donor–Acceptor Neutral Radicals Not Following the Aufbau Principle," *Nature Materials* 18 (2019): 977–984, https://doi.org/10.1038/s41563-019-0433-1.

[3] Q. Peng, A. Obolda, M. Zhang, and F. Li, "Organic Light-Emitting Diodes Using a Neutral π Radical as Emitter: The Emission from a Doublet," *Angewandte Chemie International Edition* 54 (2015): 7091–7095, https://doi.org/10.1002/anie.201500242.

[4] P. Murto, R. Chowdhury, S. Gorgon, et al., "Mesitylated Trityl Radicals, a Platform for Doublet Emission: Symmetry Breaking, Charge-Transfer States and Conjugated Polymers," *Nature Communications* 14 (2023): 4147, https://doi.org/10.1038/s41467-023-39834-2.

[5] A. Abdurahman, T. J. H. Hele, Q. Gu, et al., "Understanding the Luminescent Nature of Organic Radicals for Efficient Doublet Emitters and Pure-Red Light-Emitting Diodes," *Nature Materials* 19 (2020): 1224–1229, https://doi.org/10.1038/s41563-020-0705-9.

[6] Z. Cui, S. Ye, L. Wang, et al., "Radical-Based Organic Light-Emitting Diodes with Maximum External Quantum Efficiency of 10.6%," *The Journal of Physical Chemistry Letters* 9 (2018): 6644–6648, https://doi.org/10.1021/acs.jpclett.8b03019.

[7] X. Ai, E. W. Evans, S. Dong, et al., "Efficient Radical-Based Light-Emitting Diodes with Doublet Emission," *Nature* 563 (2018): 536–540, https://doi.org/10.1038/s41586-018-0695-9.

[8] H.-H. Cho, S. Gorgon, G. Londi, et al., "Efficient Near-Infrared Organic Light-Emitting Diodes with Emission from Spin Doublet Excitons," *Nature Photonics* 18 (2024): 905–912, https://doi.org/10.1038/s41566-024-01458-3.

[9] H.-H. Cho, S. Gorgon, H.-C. Hung, et al., "Efficient and Bright Organic Radical Light-Emitting Diodes with Low Efficiency Roll-Off," *Advanced Materials* 35 (2023): 2303666, https://doi.org/10.1002/adma.202303666.

[10] H.-H. Cho, S. Kimura, N. C. Greenham, et al., "Near-Infrared Light-Emitting Diodes from Organic Radicals with Charge Control," *Advanced Optical Materials* 10 (2022): 2200628, https://doi.org/10.1002/adom.202200628.

[11] P. Ghosh, A. M. Alvertis, R. Chowdhury, et al., "Decoupling Excitons from High-Frequency Vibrations in Organic Molecules," *Nature* 629 (2024): 355–362, https://doi.org/10.1038/s41586-024-07246-x.

[12] F. Li, A. J. Gillett, Q. Gu, et al., "Singlet and Triplet to Doublet Energy Transfer: Improving Organic Light-Emitting Diodes with Radicals," *Nature Communications* 13 (2022): 2744, https://doi.org/10.1038/s41467-022-29759-7.

[13] Y.-J. Yu and F. Li, "Perspective on Doublet Electroluminescence from Organic Radicals," *Applied Physics Letters* 126 (2025): 100503, https://doi.org/10.1063/5.0246006.

[14] Q. Gu, S. Gorgon, A. S. Romanov, F. Li, R. H. Friend, and E. W. Evans, "Fast Transfer of Triplet to Doublet Excitons from Organometallic Host to Organic Radical Semiconductors," *Advanced Materials* 36 (2024): 2402790, https://doi.org/10.1002/adma.202402790.

[15] C. Lu, E. Cho, K. Wan, et al., "Achieving Nearly 100% Photoluminescence Quantum Efficiency in Organic Radical Emitters by Fine-Tuning the Effective Donor-Acceptor Distance," *Advanced Functional Materials* 34 (2024): 2314811, https://doi.org/10.1002/adfm.202314811.

[16] C. Lu, E. Cho, Z. Cui, et al., "Towards Efficient and Stable Donor-Acceptor Luminescent Radicals," *Advanced Materials* 35 (2023): 2208190, https://doi.org/10.1002/adma.202208190.

[17] Y. Hattori, T. Kusamoto, and H. Nishihara, "Luminescence, Stability, and Proton Response of an Open-Shell (3,5-Dichloro-4-pyridyl)bis(2,4,6-trichlorophenyl)methyl Radical," *Angewandte Chemie International Edition* 53 (2014): 11845–11848, https://doi.org/10.1002/anie.201407362.

[18] J. Ding, H.-H. Cho, C. Lu, et al., "Enabling Efficient Deep Near-Infrared Radical Electroluminescence Around 900 nm via Donor-Mediated Vibronic Suppression," *Advanced Optical Materials* 14 (2026): e71228, https://doi.org/10.1002/adom.71228.

[19] Z. Cui, A. Abdurahman, X. Ai, and F. Li, "Stable Luminescent Radicals and Radical-Based LEDs with Doublet Emission," *CCS Chemistry* 2 (2020): 1129–1145, https://doi.org/10.31635/ccschem.020.202000210.

[20] J. M. Hudson, T. J. H. Hele, and E. W. Evans, "Efficient Light-Emitting Diodes from Organic Radicals with Doublet Emission," *Journal of Applied Physics* 129 (2021): 180901, https://doi.org/10.1063/5.0047636.

[21] C. Murawski, K. Leo, and M. C. Gather, "Efficiency Roll-Off in Organic Light-Emitting Diodes," *Advanced Materials* 25 (2013): 6801–6827, https://doi.org/10.1002/adma.201301603.

[22] D. Yokoyama, H. Sasabe, Y. Furukawa, C. Adachi, and J. Kido, "Molecular Stacking Induced by Intermolecular C–H···N Hydrogen Bonds Leading to High Carrier Mobility in Vacuum-Deposited Organic Films," *Advanced Functional Materials* 21 (2011): 1375–1382, https://doi.org/10.1002/adfm.201001919.

[23] H. Sasabe, D. Tanaka, D. Yokoyama, et al., "Influence of Substituted Pyridine Rings on Physical Properties and Electron Mobilities of 2-Methylpyrimidine Skeleton-Based

Electron Transporters," *Advanced Functional Materials* 21 (2011): 336–342, https://doi.org/10.1002/adfm.201001252.

[24] T.-L. Wu, M.-J. Huang, C.-C. Lin, et al., "Diboron Compound-Based Organic Light-Emitting Diodes with High Efficiency and Reduced Efficiency Roll-Off," *Nature Photonics* 12 (2018): 235–240, https://doi.org/10.1038/s41566-018-0112-9.

[25] N. B. Kotadiya, P. W. M. Blom, and G.-J. A. H. Wetzelaer, "Efficient and Stable Single-Layer Organic Light-Emitting Diodes Based on Thermally Activated Delayed Fluorescence," *Nature Photonics* 13 (2019): 765–769, https://doi.org/10.1038/s41566-019-0488-1.

[26] H.-H. Cho, D. G. Congrave, A. J. Gillett, et al., "Suppression of Dexter Transfer by Covalent Encapsulation for Efficient Matrix-Free Narrowband Deep Blue Hyperfluorescent OLEDs," *Nature Materials* 23 (2024): 519–526, https://doi.org/10.1038/s41563-024-01812-4.

[27] H.-H. Cho, D. G. Congrave, S. Gorgon, V. Riesgo-Gonzalez, R. H. Friend, and H. Bronstein, "TADF Host Engineering for Improved Pure Blue Matrix-Free Hyperfluorescent OLEDs with Ultranarrow Emission," *Advanced Optical Materials* 13 (2025): 2500246, https://doi.org/10.1002/adom.202500246.

[28] V. R. Nikitenko, V. I. Arkhipov, Y.-H. Tak, J. Pommerehne, H. Bässler, and H. H. Hörhold, "The Overshoot Effect in Transient Electroluminescence from Organic Bilayer Light Emitting Diodes: Experiment and Theory," *Journal of Applied Physics* 81 (1997): 7514–7525, https://doi.org/10.1063/1.365293.

[29] C. Weichsel, L. Burtone, S. Reineke, et al., "Storage of Charge Carriers on Emitter Molecules in Organic Light-Emitting Diodes," *Physical Review B* 86 (2012): 075204, https://doi.org/10.1103/PhysRevB.86.075204.

[30] Y.-J. Pu, R. Satake, Y. Koyama, et al., "Absence of Delayed Fluorescence and Triplet–Triplet Annihilation in Organic Light Emitting Diodes with Spatially Orthogonal Bianthracenes," *Journal of Materials Chemistry C* 7 (2019): 2541–2547, https://doi.org/10.1039/C8TC05817B.

[31] J.-Y. Huang, J.-H. Lee, Y.-R. Wu, et al., "Revealing the Mechanism of Carrier Transport in Host-Guest Systems of Organic Materials with a Modified Poisson and Drift-Diffusion Solver," *Physical Review Materials* 4 (2020): 125602, https://doi.org/10.1103/PhysRevMaterials.4.125602.

[32] J.-Y. Huang, H.-C. Hung, K.-C. Hsu, et al., "Numerical Analysis and Optimization of a Hybrid Layer Structure for Triplet–Triplet Fusion Mechanism in Organic Light-Emitting Diodes," *Advanced Theory and Simulations* 6 (2023): 2200633, https://doi.org/10.1002/adts.202200633.

[33] T.-J. Kung, J.-Y. Huang, J.-J. Huang, et al., "Modeling of Carrier Transport in Organic Light Emitting Diode with Random Dopant Effects by Two-Dimensional Simulation," *Optics Express* 25 (2017): 25492–25503, https://doi.org/10.1364/OE.25.025492.